Supplementary information

Sub-cycle transient scanning tunneling spectroscopy with visualization of enhanced terahertz near-field

Shoji Yoshida[1], Hideki Hirori[2], Takehiro Tachizaki[3], Katsumasa Yoshioka[4], Yusuke Arashida[4],

Zi-Han Wang[1], Yasuyuki Sanari[2], Osamu Takeuchi[1], Yoshihiko Kanemitsu[2], and Hidemi Shigekawa[1]

[1]Faculty of Pure and Applied Sciences, University of Tsukuba, Tsukuba 305-8573, Japan

[2]Institute for Chemical Research, Kyoto University, Uji, Kyoto, 611-0011

[3]Department of Optical and Imaging Science and Technology, Tokai University, Hiratsuka-shi, Kanagawa, 259-1292, Japan

[4]Department of Physics, Graduate School of Engineering, Yokohama National University, Yokohama, 240-8501, Japan
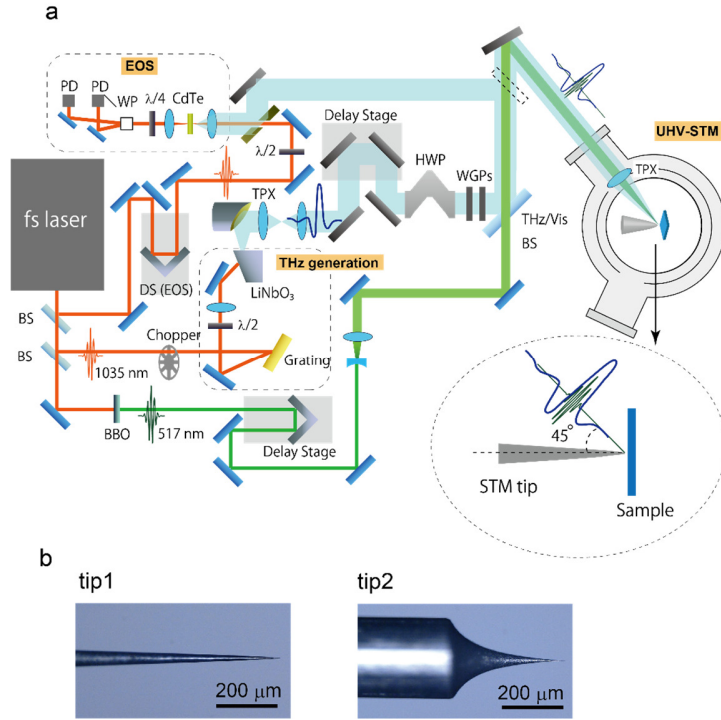
Figure S1. Schematic illustration of the experimental setup combining the THz laser system and STM. **a**, BS: beam splitter, DS: delay stage, PD: photodetector, PL: polarizer, WP: Wollaston prism, EOS: electro-optic sampling, TPX: polymethylpentene lens. HWP: half-wave plate. EOS utilizes the fact that when a THz pulse and a shorter IR pulse irradiate a crystal such as CdTe, the polarization plane of the IR light rotates by an amount depending on the intensity of the simultaneously existing THz electric field. Namely, the THz electric field waveform can be obtained by measuring the angle of the rotation of IR light while varying the delay time t_d between both pulses. The THz pulse was generated by irradiating the $LiNbO_3$ crystal with IR pulse light (1034 nm, 300 fs, 1 MHz), which was almost a single cycle with a first peak of 1 ps width, as shown in Fig. 2g. The probe light used for photoemission measurement was generated by converting IR light into a second harmonic wave (517 nm) with a BBO crystal. The relationship between the incident light and the sample is shown in the lower right figure. Both the optical pulses were focused onto the STM tunnel junction by TPX lens placed in the UHV chamber. The focal length is 100 mm and the incident angle was 45°. The spot size of the IR light was 10 μm and its position (on the probe) was scanned in steps of 45 μm with a piezo mirror. The base pressure of the STM chamber was 1×10^{-7} Pa and the current noise level was 4 fA/√(Hz). **b**, Two types of STM tips.

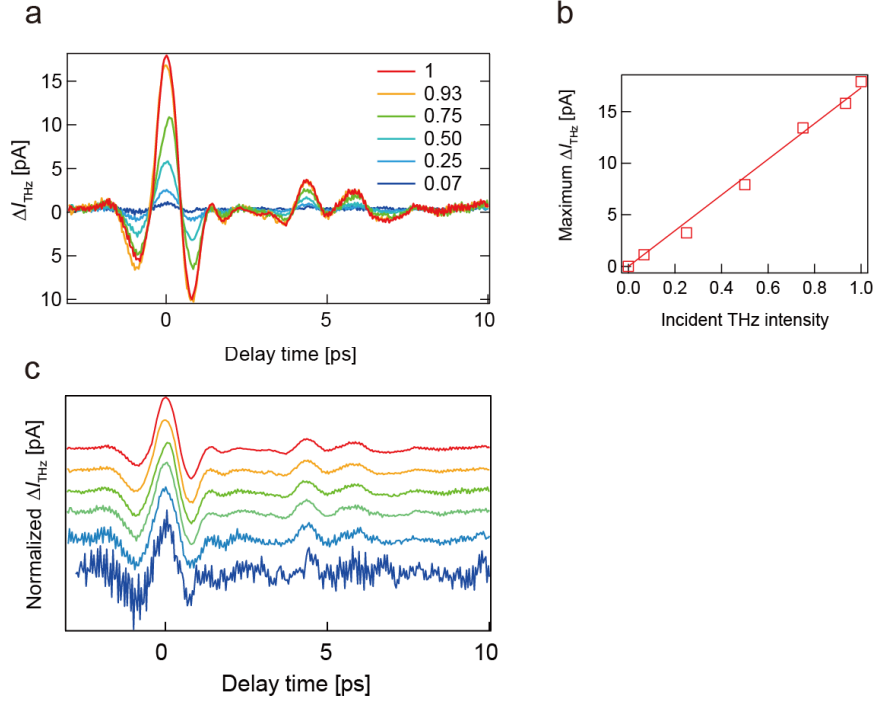**Figure S2**. Dependence of THz waveform at tip apex on electric field strength. **a**, Change in the THz near-field waveform at the tip apex (ΔI_{THz}). The intensity of the THz near field changed according to the change with the intensity of the incident THz electric field. **b**, Dependence of the maximum (zero-delay) peak value of the waveform in **a** on the electric field strength, showing a linear relationship. **c**, Normalized electric field in **a**. Corresponding waveforms in **a** and **c** are shown in the same color. A similar waveform was observed regardless of the incident electric field strength.
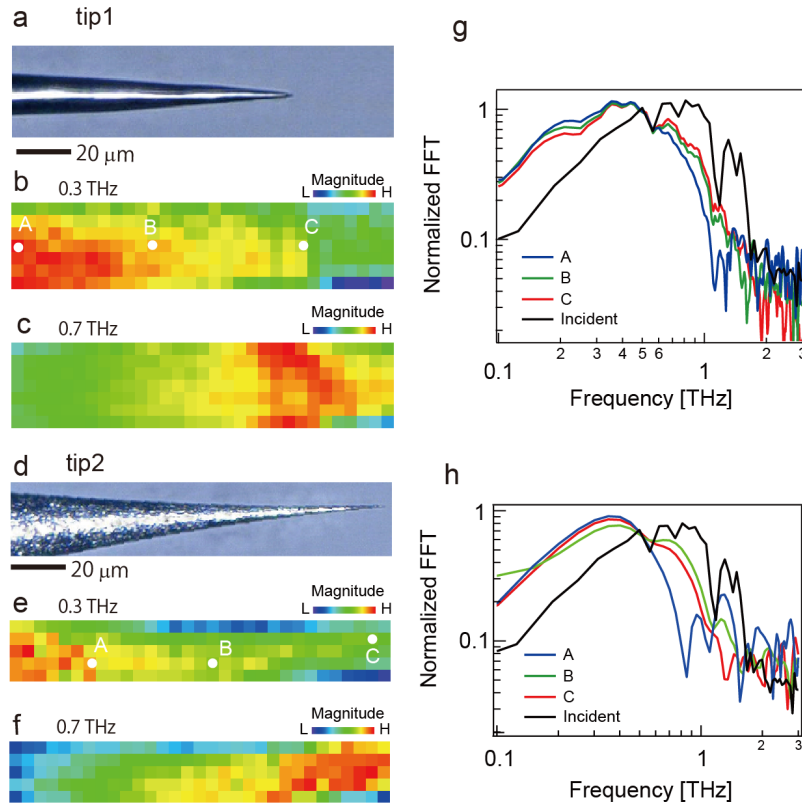
Figure S3. Frequency dependence of the THz electric field modulated by the two types of nanotips. **a**, Optical micrograph of tip 1. **b**, **c**, Maps of electric field strength for frequencies of 0.3 and 0.7 THz, respectively. **d**, Optical micrograph of tip 2. **e**, **f**, Maps of electric-field strength for frequencies of 0.3 and 0.7 THz, respectively. **g**, **h**, Fourier spectra of the electric-field strength obtained at A, B, and C for tips 1 and 2, respectively. The measurement conditions were the same as those for Fig. 2. All Fourier spectra of the near field differ strongly from that of the incident THz electric field. When the incident THz waveform has components centered around 1 THz, the near-field waveform is shifted to the lower-frequency side (redshift) and becomes centered around 0.5 THz. The change in the bandwidth can be explained to some extent by the dipole. High frequency components are reduced by the factor of $1/f$ (f: frequency), which was experimentally confirmed by NSOM[1]. To investigate the details of the electric field distribution around the metal tip, we performed finite different time domain (FDTD) calculation and the results are shown in Fig. S4. The experimental results were reproduced well.
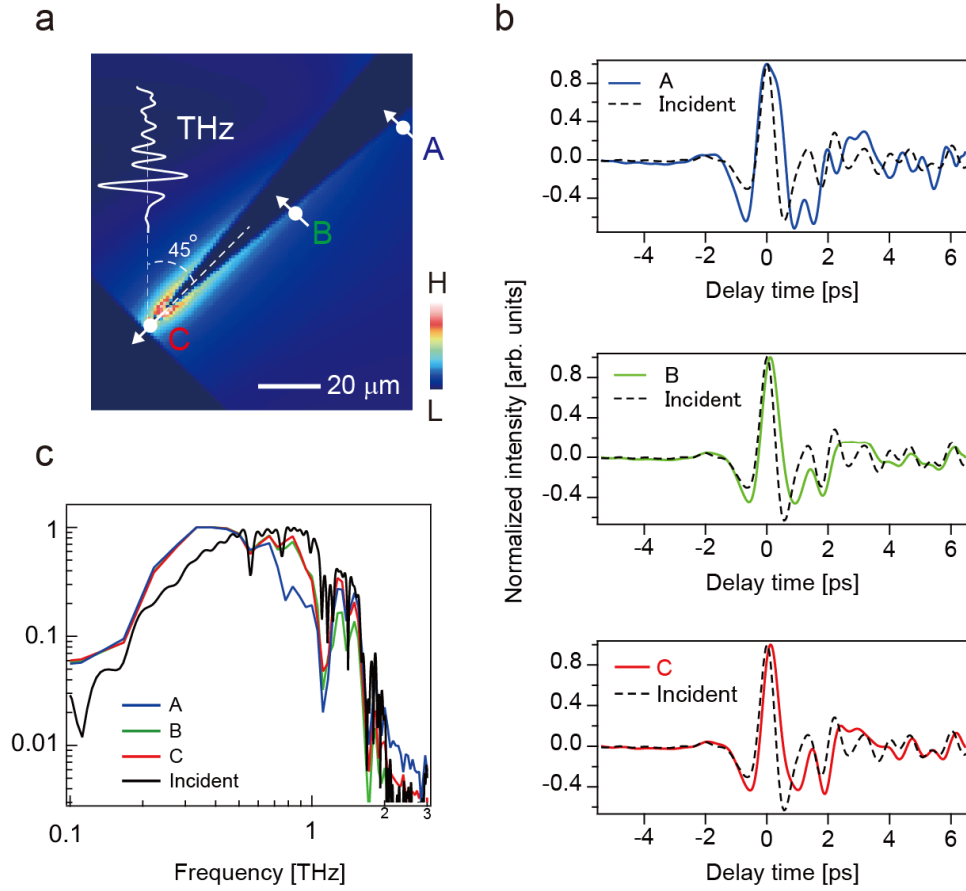
Figure S4. FDTD Simulations of near field. **a**, Calculation configuration consisting of the W tip (tip 1) and graphite sample, and the spatial distribution of the electric field at the Fourier component of 0.7 THz. **b**, Waveforms simulated at A, B, and C shown in **a**. **c**, Frequency dependence of the THz electric fields obtained from the waveforms in **b**. In the calculation, the complex dielectric function for the metal tip and graphite sample is given by $\varepsilon = \varepsilon_\infty + i/\varepsilon_0 \rho \omega$, where $\varepsilon_\infty = 1$, ε_0 is the vacuum permittivity, and the conductivity σ for the tungsten tip and graphite sample are 52.8 nΩ·m and 0.4 μΩ·m, respectively. The incident angle of THz pulse is 45 degrees against the metal tip.
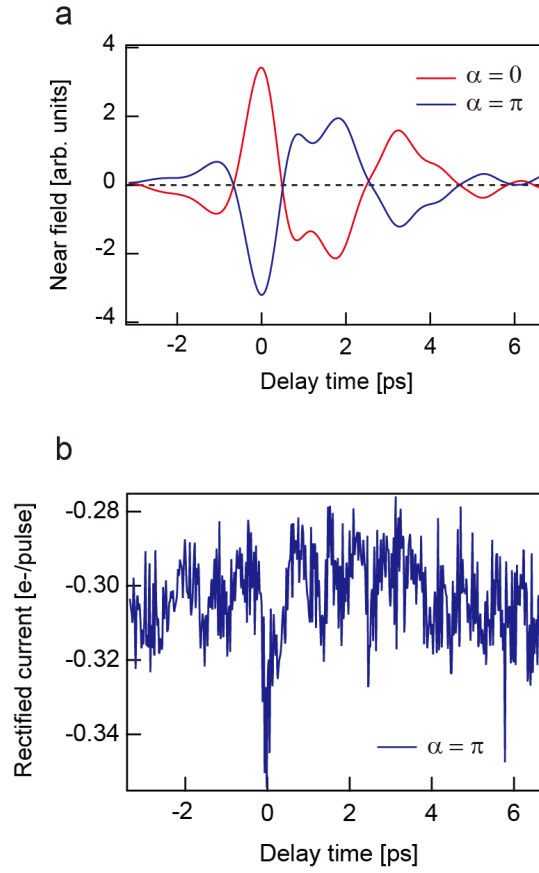
a

b

Figure S5. Measurement results for HOPG. **a**. Tip-enhanced near-field waveform obtained by photoelectron measurement. **b**. Spectrum obtained in tunnel regime obtained for $\alpha = \pi$ ($V_S = 2$ mV, $I_T = 2$ pA, $I_{IR} = 3.8$ mJ/cm^2, $f_{rep} = 1$ MHz). A similar THz near-field profile was also measured on the HOPG sample; however, I_{THz} was very low compared to that for Bi$_2$Se$_3$ and the signal was faintly observed only for $t_d = 0$, which is considered to be caused by the weak excitation of hot electrons in HOPG. Namely, the optical transition in HOPG with the energy of the IR pulse used is limited to the π-π* transition near the K point, whereas various optical transitions are possible in Bi$_2$Se$_3$, as known from the results of photoelectron emission spectroscopy. The signal level of HOPG in this experiment was already extremely low (0.05 e^-/pulse), which is close to the detection limit of our system at present. Further improvement is necessary to investigate weak signals such as those from HOPG, and the use of a light source with an even higher repetition rate is considered to be a possible technique
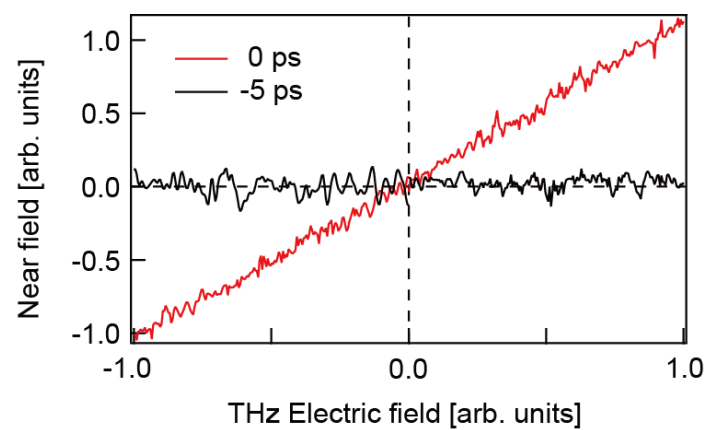
Figure S6. Relationship between tip-enhanced near field strength and THz intensity obtained by photoelectron measurement. A linear relationship similar to that in Fig. S2**b** was obtained.
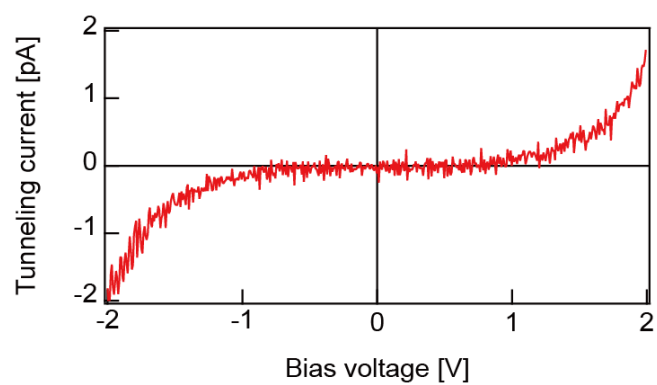
Figure S7. Tunnel spectrum of Bi$_2$Se$_3$ (V_S = 2 V, I_T = 2 pA).
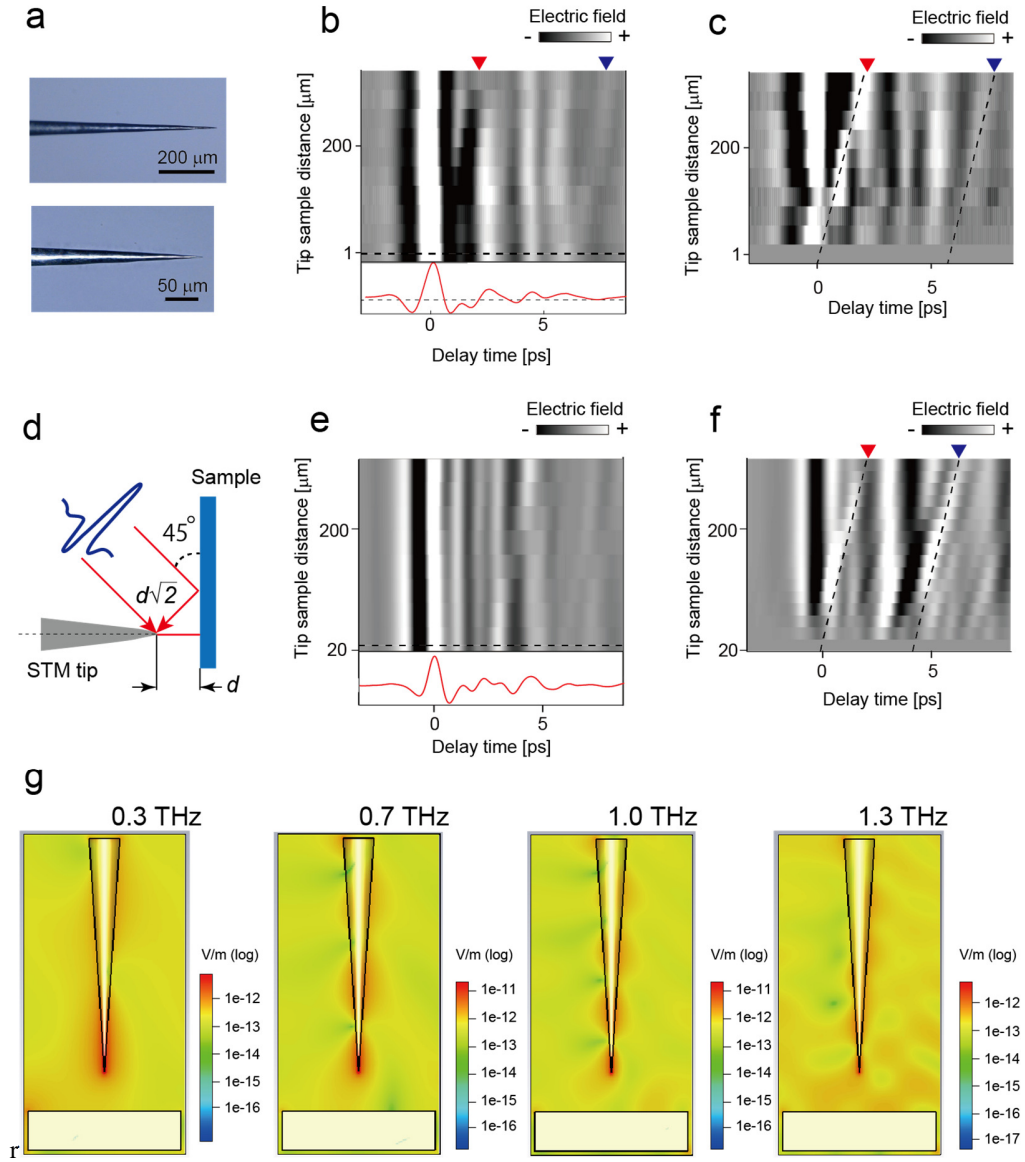
Figure S8. Tip-sample distance dependence of the near-field waveform at the tip apex.

a. Optical photograph of tip 1 used in the experiment. **b**. Tip-sample distance dependence of the near-field waveform at the tip apex (experiment). The nanotip was retracted from 1μm with steps of 36 μm, and the same measurements as in Fig. 2 were performed for each step. **c**. Tip-sample distance dependence of the near-field waveform at the tip apex in which the electric field waveforms at 1μm was subtracted from the data in **b**. **d**. Configuration used for the simulation. d represents the distance between the tip and sample, which was set to 100 μm here. **e**. Tip-sample

distance dependence of the near-field waveform at the tip apex (simulation). The nanotip was retracted from 20μm with steps of 40 μm Tip-sample distance dependence of the near-field waveform at the tip apex. **f**. Tip-sample distance dependence of the near-field waveform at the tip apex in which the electric field waveforms at 20 μm was subtracted from the data in **e**. Tip-sample distance dependence of the near-field waveform at the tip apex in which the electric field waveforms at 1μm was subtracted from the data in **d**. In **c** and **f**, some diagonal lines were exaggerated as shown by the red and black triangles and the dashed lines. Their positions are slightly different between the experiment and the simulation due to the slight difference in the waveform shown in **b** and **e**. Since the phase shift which produced the slopes corresponds to $\sqrt{2}d/c$ (d : tip-sample distance, c : the speed of light), the observed diagonal lines are considered to be the change in the delay of the arrival time of the light reflected from the sample, which is in good agreement with the effect predicted by the simulation for the STM setup in the previous paper[2]. **g**. Map of the strength of the simulated electric field at various frequencies. The effect of the standing wave exists along the tip, which, however, did not depend on the tip-sample distance, indicating that there is no clear resonance effect in this case.

As shown here, the influence of reflection appears at a far place, but the THz waveform at the tip apex hardly changes within the distance of 1 μm.Therefore, it is considered reasonable to use the THz electric field shown in Fig. 3d for the analysis in the tunnel region in Fig. 3g.

Reference

(1)   Wang, K.; Mittleman, D. M.; Van Der Valk, N. C. J.; Planken, P. C. M. Antenna Effects in Terahertz Apertureless Near-Field Optical Microscopy. *Appl. Phys. Lett.* **2004**, *85*, 2715–2717.

(2)   Nguyen, P. H.; Rathje, C.; Hornig, G. J.; Jelic, V.; Ropers, C.; Hegmann, F. A. Coupling Terahertz Pulses to a Scanning Tunneling Microscope. *Phys. Canada.* **2015**, *71*, 157–160.